Promoter-anchored chromatin interactions predicted from genetic analysis of epigenomic data

Yang Wu[1,7], Ting Qi[1,7], Huanwei Wang[1], Futao Zhang[1], Zhili Zheng[1,2], Jennifer E. Phillips-Cremins[3], Ian J. Deary[4,5], Allan F. McRae[1], Naomi R. Wray[1,6], Jian Zeng[1], Jian Yang[1,2,6,*]

[1] Institute for Molecular Bioscience, The University of Queensland, Brisbane, Queensland 4072, Australia

[2] Institute for Advanced Research, Wenzhou Medical University, Wenzhou, Zhejiang 325027, China

[3] Department of Bioengineering, University of Pennsylvania, Philadelphia, PA 19104, USA

[4] Centre for Cognitive Ageing and Cognitive Epidemiology, University of Edinburgh, Edinburgh EH8 9JZ, UK

[5] Department of Psychology, University of Edinburgh, Edinburgh EH8 9JZ, UK

[6] Queensland Brain Institute, The University of Queensland, Brisbane, Queensland 4072, Australia

[7] These authors contributed equally to this work.

[*] Correspondence: Jian Yang (jian.yang.qt@gmail.com)

Abstract

Promoter-anchored chromatin interactions (PAIs) play a pivotal role in transcriptional regulation. Current high-throughput technologies for detecting PAIs, such as promoter capture Hi-C, are not scalable to large cohorts. Here, we present an analytical approach that uses summary-level data from cohort-based DNA methylation (DNAm) quantitative trait locus (mQTL) studies to predict PAIs. Using mQTL data from human peripheral blood (n=1,980), we predicted 34,797 PAIs which showed strong overlap with the chromatin contacts identified by previous experimental assays. The promoter-interacting DNAm sites were enriched in enhancers or near expression QTLs. Genes whose promoters were involved in PAIs were more actively expressed, and gene pairs with promoter-promoter interactions were enriched for co-expression. Integration of the predicted PAIs with GWAS data highlighted interactions among 601 DNAm sites associated with 15 complex traits. This study demonstrates the use of mQTL data to predict PAIs and provides insights into the role of PAIs in complex trait variation.

Introduction

Genome-wide association studies (GWASs) in the past decade have identified tens of thousands of genetic variants associated with human complex traits (including common diseases) at a stringent genome-wide significance level[1,2]. However, most of the trait-associated variants are located in non-coding regions[3,4], and the causal variants as well as their functional roles in trait etiology are largely unknown. One hypothesis is that the genetic variants affect the trait through genetic regulation of gene expression[4]. Promoter-anchored chromatin interaction (PAI)[5,6] is a key regulatory mechanism whereby non-coding genetic variants alter the activity of cis-regulatory elements and subsequently regulate the expression levels of the target genes. Therefore, a genome-wide map of PAIs is essential to understand transcriptional regulation and the genetic regulatory mechanisms underpinning complex trait variation.

High-throughput experiments, such as Hi-C[7] and ChIA-PET (chromatin interaction analysis by paired-end tag sequencing)[8], have been developed to detect chromatin interactions by a massively parallelized assay of ligated DNA fragments. Hi-C is a technique based on chromosome conformation capture (3C)[9] to quantify genome-wide interactions between genomic loci that are close in three-dimensional (3D) space, and ChIA-PET is a method that combines ChIP-based methods[10] and 3C. However, these high-throughput assays are currently not scalable to population-based cohorts with large sample sizes because of the complexity of generating a DNA library for each individual (tissue or cell line) and the extremely high sequencing depth needed to achieve high detection resolution[11]. On the other hand, recent technological advances have facilitated the use of epigenomic marks to infer the chromatin state of a specific genomic locus and further to predict the transcriptional activity of a particular gene[12,13]. There have been increasing interests in the use of epigenomic data (e.g., DNA methylation (DNAm) and/or histone modification) to infer chromatin interactions[14-17]. These analyses, however, rely on individual-level chromatin accessibility data often only available in small samples[14,16], and it is not straightforward to use the predicted chromatin interactions to interpret the variant-trait associations identified by GWAS.

In this study, we proposed an analytical approach to predict chromatin interaction by detecting the association between DNAm levels of two CpG sites due to the same set of genetic variants (i.e., pleiotropic association between DNAm sites). This can be achieved because if the methylation levels (unmethylated, partly methylated or fully methylated) of a pair of relatively distal CpG sites covary across individuals and such covariation is not (or at least not completely) caused by environmental or experimental factors (evidenced by the sharing of a common set of causal genetic variants in cis) (**Fig. 1b**), it is very likely that the two genomic regions interact (having

contacts or functional links because of their close physical proximity in 3D space). Our analytical approach was based on two recently developed methods, i.e., the summary-data–based Mendelian randomization (SMR) test and the test for heterogeneity in dependent instruments (HEIDI)[18], which are often used in combination to detect pleiotropic association between a molecular phenotype (e.g. gene expression or DNA methylation) and a complex trait[18] or between two molecular phenotypes[19]. The SMR & HEIDI approach only requires summary-level data from DNA methylation quantitative trait locus (mQTL) studies, providing the flexibility of using mQTL data from studies with large sample sizes to ensure efficient power. Since the proposed method is based on cohort-based genetic data, it also allows us to integrate the predicted chromatin interactions with GWAS results to understand the genetic regulatory mechanisms for complex traits. In this study, we analyzed mQTL summary data from a meta-analysis of two cohort-based studies on 1,980 individuals with DNAm levels measured by Illumina 450K methylation arrays and SNP data from SNP-array-based genotyping followed by imputation to the 1000 Genome Project (1KGP) reference panels[19,20].

Results

Predicting promoter-anchored chromatin interactions using mQTL data

As described above, our underlying hypothesis was that if the variation between people in DNAm levels of two relatively distal CpG sites are associated due to the same set of causal genetic variants (**Fig. 1b**), then it is very likely that these two chromatin regions have contacts or functional links because of their close physical proximity in 3D space. Hence, we set out to predict promoter-anchored chromatin interactions (PAIs) from mQTL data. We applied the SMR & HEIDI approach[18] to test for pleiotropic associations of a DNAm site in the promoter region of a gene with all the other DNAm sites within 2 Mb of the focal promoter in either direction (excluding those in the focal promoter) using mQTL summary data from peripheral blood samples (**Fig. 1**, **Fig. S1** and **Methods**). Therefore, our analysis was a scan for genomic regions that are functionally associated with promoter regions likely because of chromatin contacts or close physical proximity in 3D space. Note that we limited the analysis to a 2 Mb window because chromatin interactions between genomic sites more than 2 Mb apart are rare[21], because summary data from epigenetic QTL studies are often only available for genetic variants in cis-regions, and because it reduces the computational and multiple testing burdens. The mQTL summary data were generated from a meta-analysis of two mQTL data sets from McRae et al. (n = 1,980)[19,20]. The mQTL effects were in standard deviation (SD) units of DNAm levels. In the SMR analysis, the promoter DNAm site was used as the "exposure" and each of the other DNAm sites in the region was used as the "outcome" (**Fig. 1**). For exposure probes, we included in the SMR analysis only the DNAm sites with at least one cis-mQTL (SNPs within 2 Mb of the CpG site associated with variation in DNAm level) at P_{mQTL}

108 $< 5 \times 10^{-8}$. We used such a stringent significance level because a basic assumption of Mendelian
109 randomization is that the SNP instrument needs to be strongly associated with the exposure[22,23].
110 There were 90,749 DNAm probes with at least one cis-mQTL at $P_{mQTL} < 5 \times 10^{-8}$, 28,732 of which
111 were located in promoters annotated based on data from blood samples of the Roadmap
112 Epigenomics Mapping Consortium (REMC)[13]. We used the 1KGP-imputed Health and Retirement
113 Study (HRS)[24] data as a reference sample for linkage disequilibrium (LD) estimation to perform
114 the HEIDI test, which was used to reject SMR associations between DNAm sites not driven by the
115 same set of causal variants (called linkage model in Zhu et al.[18]). In total, we identified 34,797 PAIs
116 between pairwise DNAm sites that passed the SMR test ($P_{SMR} < 1.76 \times 10^{-9}$ based on a Bonferroni
117 correction for multiple tests) and were not rejected by the HEIDI test ($P_{HEIDI} > 0.01$; see Wu et al.[19]
118 for the justification of the use of this HEIDI threshold *P* value). The significant PAIs comprised of
119 21,787 unique DNAm sites, among which 10,249 were the exposure probes in promoter regions
120 of 4,617 annotated genes. Most of the DNAm sites in promoters showed pleiotropic associations
121 with multiple DNAm sites (mean = 4) (**Fig. S2a**). The distances between 95% of the pairwise
122 interacting DNAm sites were less than 500 Kb (mean = 79 Kb and median = 23 Kb). Only ~0.7%
123 of the predicted PAIs were between DNAm sites greater than 1 Mb apart (**Fig. S2b**). The summary
124 statistics of the predicted PAIs are publicly available through the M2Mdb Shiny online application
125 (**URLs**).
126
127 **Overlap of the predicted PAIs with chromatin contacts identified from experimental assays**
128 We first examined whether the predicted PAIs are consistent with chromatin contacts identified
129 by experimental assays, such as Hi-C[21] and promoter captured Hi-C (PCHi-C)[5]. While the majority
130 of experimental assays are measured in primary cell lines, topological associated domains (TADs)
131 annotated from Hi-C are relatively conserved across cell types[25]. We therefore tested the overlap
132 of our predicted PAIs with the TADs identified from recent Hi-C and PCHi-C studies[5,21,26] (see
133 **Supplementary Table 1** for a full list of data sets from experimental assays used in this study).
134 We found that 22,024 (63.3%) of the predicted PAIs were between DNAm sites located in the
135 TADs identified by Rao et al. using Hi-C in the GM12878 cell lines[21], 27,200 (78.2%) in those by
136 Dixon et al. using Hi-C in embryonic stem cells[26], and 27,716 (79.7%) in those by Javierre et al.
137 using PCHi-C in primary hematopoietic cells[5]. These overlaps with Hi-C and PCHi-C data were
138 significantly higher than expected by chance ($P < 0.001$ for all the three Hi-C/PCHi-C data sets; **Fig.**
139 **2a-c**). Note that the *P* value was computed by comparing the observed number to a null
140 distribution generated by resampling the same number of DNAm pairs at random from distance-
141 matched DNAm pairs included in the SMR analysis (**Methods**); the *P* value was truncated at 0.001
142 due to the finite number of resampling. One example was the *MAD1L1* locus (a ~450 Kb region)
143 on chromosome 7 (**Fig. 2d** and **Fig. 2e**) where there were a large number of predicted PAIs highly

144 consistent with TADs identified by Hi-C from the Rao et al. study[21]. There were also scenarios
145 where the predicted PAIs were not aligned well with the TAD data. For example, 107 of the 183
146 predicted PAIs at the *RPS6KA2* gene locus did not overlap with the TADs identified by Hi-C from
147 the Rao et al. study[21] (**Fig. S3a**). These predicted interactions, however, are very likely to be
148 functional as indicated by our subsequent analysis with GWAS and omics data (see below).
149 Additionally, the predicted PAIs were slightly enriched for the Hi-C loops identified from Rao *et*
150 *al.*[21] (1.49-fold, $P < 0.001$, m = 130; **Fig. 3a**) and the *POLR2A* ChIA-PET loops from the ENCODE[27]
151 project (1.44-fold, $P < 0.001$, m = 2,315; **Fig. 3b**), although the numbers of overlaps were small.
152 One notable example was the *GNB1* locus where the predicted PAI between the promoter region
153 of *GNB1* and an enhancer nearby is consistent with the enhancer-promoter interaction identified
154 by both Hi-C from Rao *et al.*[21] and PCHi-C from Jung *et al.*[28] in the GM12878 cell lines (**Fig. S4**).
155

156 **Comparison with other prediction methods**

157 To assess the performance of our PAI prediction method, we compared it with two state-of-the-
158 art approaches of this kind, i.e., the correlation-based method used in Gate *et al.*[29] and the pairwise
159 hierarchical model (PHM) method developed by Kumasaka *et al.*[17], using the DNAm data
160 described above or the chromatin accessibility data (measured by Assay for Transposase-
161 Accessible Chromatin using sequencing (ATAC-seq)) from Kumasaka *et al.*[17]. We used a recently
162 released chromatin interaction data (PCHi-C loops) generated by Jung *et al.*[28] in GM12878 cell
163 lines for validation, and quantified the enrichment of the predicted interactions in the PCHi-C
164 loops defined based on a range of PCHi-C *P* value thresholds. We chose the PCHi-C data from Jung
165 *et al.* because the *P* values of all the tested loops are available and because compared to other Hi-
166 C data sets, chromatin interactions identified in GM12878 cell lines may be more relevant to the
167 predicted PAIs in whole blood. We computed the fold enrichment of the predicted interactions by
168 the three methods in the PCHi-C loops by a 2×2 contingency table and used the Fisher's exact
169 test to assess the statistical significance of the enrichment (**Methods**). The results showed that
170 our predicted PAIs using either DNAm or chromatin accessibility data were highly enriched in the
171 PCHi-C loops and that the fold enrichment increased with the increase of the significance level
172 used to claim the PCHi-C loops (**Fig. 3c**), consistent with the observation from previous work that
173 Hi-C loops with lower *P* values are more reproducible between biological replicates[30]. Our SMR &
174 HEIDI method outperformed the correlation-based method using either DNAm or chromatin
175 accessibility data, as evidenced by the larger fold enrichment of our method compared to the
176 correlation-based method at all the PCHi-C significance levels (**Fig. 3c**). We also compared the
177 predicted PAIs with the interactions identified from the PHM approach[17] using the chromatin
178 accessibility data. Of the 15,487 interactions identified by the PHM approach, 10,416 were tested
179 in our SMR & HEIDI analysis; 98.4% were replicated at a nominal significance level ($P_{SMR} < 0.05$

180 and $P_{HEIDI} > 0.01$), and 36% were significant after multiple testing correction ($P_{SMR} < 4.8 \times 10^{-6}$
181 (0.05/10,416) and $P_{HEIDI} > 0.01$). While the PHM approach requires individual-level genotype and
182 chromatin accessibility data and is less computationally efficient due to the use of Bayesian
183 hierarchical model, our SMR & HEIDI method that requires only summary-level data is more
184 flexible and can be potentially applied to all epigenetic QTL data.
185
186 **Enrichment of the predicted PAIs in functional annotations**
187 To investigate the functional role of the DNAm sites that showed significant interactions with the
188 DNAm sites in promoter regions (called promoter-interacting DNAm sites or PIDSs hereafter), we
189 conducted an enrichment analysis of the PIDSs (m = 14,361) in 14 main functional annotation
190 categories derived from the REMC blood samples (**Methods**). The fold-enrichment was computed
191 as the proportion of PIDSs in a functional category divided by the mean of a null distribution
192 generated by resampling variance-matched "control" probes at random from all the outcome
193 probes used in the SMR analysis. We found a significant enrichment of PIDSs in enhancers (fold-
194 enrichment=2.17 and $P_{enrichment} < 0.001$), repressed Polycomb regions (fold-enrichment=1.56 and
195 $P_{enrichment} < 0.001$), primary DNase (fold-enrichment=1.43 and $P_{enrichment} < 0.001$) and bivalent
196 promoters (fold-enrichment=1.12 and $P_{enrichment} < 0.001$) and a significant underrepresentation in
197 transcription starting sites (fold-enrichment=0.21 and $P_{enrichment} < 0.001$), quiescent regions (fold-
198 enrichment=0.74 and $P_{enrichment} < 0.001$), promoters around transcription starting sites (fold-
199 enrichment=0.77 and $P_{enrichment} < 0.001$), and transcribed regions (fold-enrichment=0.90 and
200 $P_{enrichment} < 0.001$) in comparison with the control probes (**Fig. 4a** and **Fig. 4b**). On one hand, the
201 enrichment test is not biased by the fact that the Illumina 450K methylation array probes are
202 preferentially distributed towards certain genomic regions (e.g., promoters; **Fig. 4a**) because it
203 tests against control probes sampled from probes on the array rather than random genomic
204 positions. On the other hand, however, this test is over conservative because the control probes
205 are enriched in certain functional genomic regions (**Fig. S5a**) and can possible contain some of
206 the PIDSs, which may explain the relatively small fold enrichments observed above. The depletion
207 of PIDSs in promoters was due to the exclusion of outcome probes from the focal promoters
208 (**Methods**; **Fig. S5b**). In addition, a large proportion (~18%) of the predicted PAIs were promoter-
209 promoter interactions (PmPmI), consistent with the results from previous studies[5,31] that PmPmI
210 were widespread.
211
212 **Relevance of the predicted PAIs with gene expression**
213 We then turned to test whether pairwise genes with significant PmPmI were enriched for co-
214 expression. We used gene expression data (measured by Transcript Per Kilobase Million mapped
215 reads or TPM) from the blood samples of the Genotype-Tissue Expression (GTEx) project[32] and

computed the Pearson correlation of expression levels across individuals between pairwise genes (r_P). To assess the statistical significance of the enrichment, we compared the observed mean Pearson correlation of all the significant PmPmI gene pairs (m = 2,236) to a null distribution of mean Pearson correlation values, generated by resampling a set of distance-matched control gene pairs either from the genes whose promoters were involved in the SMR analysis or from all genes. The mean correlation for the significant PmPmI gene pairs ($\bar{r}_P$) was 0.367, significantly ($P < 0.001$) higher than that for the control gene pairs sampled either from the genes whose promoters were involved in SMR (mean $\bar{r}_P$ = 0.292; **Fig. 4c**) or from all genes (mean $\bar{r}_P$ = 0.156; **Fig. 4c**), suggesting that pairwise genes with PmPmI are more likely to be co-expressed.

We also tested whether genes whose promoters were involved in significant PAI (called Pm-PAI genes hereafter, **Fig. 1**) were expressed more actively than the same number of control genes randomly sampled from the genes whose promoters were involved in SMR or from all genes. Similar to the analysis above, we used the gene expression data (measured by TPM) from the blood samples of the GTEx project and tested the enrichment of Pm-PAI genes in different expression level groups (**Methods**). In comparison to the control sets sampled from the genes whose promoters were involved in SMR, Pm-PAI genes were significantly overrepresented ($P < 0.001$) among the group of genes with the highest expression levels and significantly underrepresented ($P < 0.001$) among genes that were not actively expressed (median TPM < 0.1) (**Fig. 4d**). These results implicate the regulatory role of the PIDSs in transcription and their asymmetric effects on gene expression. The enrichment was much stronger if the control sets were sampled from all genes (**Fig. S6a**). We also performed a similar enrichment analysis (testing against the control sets sampled from all genes) for the predicted target genes from the PCHi-C data from Jung *et al.*[28]. There was a significant enrichment of the PCHi-C target genes in the active gene groups, but the fold enrichment was slightly smaller than that of the Pm-PAI genes (**Fig. S6**), suggesting that PAIs could be more functionally relevant than PCHi-C loops.

Enrichment of eQTLs in the PIDS regions

We have shown that the PIDSs are located in regions enriched with regulatory elements (e.g., enhancers) (**Fig. 4b**) and that the Pm-PAI genes tend to have higher expression levels (**Fig. 4d**). We next investigated if genomic regions near PIDS are enriched for genetic variants associated with expression levels of the Pm-PAI genes using data from an expression QTL (eQTL) study in blood[33]. There were 11,204 independent cis-eQTLs at $P_{\mathrm{eQTL}} < 5 \times 10^{-8}$ for 9,967 genes, among which 2,019 were Pm-PAI genes (**Methods**). We mapped cis-eQTLs to a 10 Kb region centered around each PIDS (5 Kb on either side) and counted the number of cis-eQTLs associated with expression levels of the corresponding Pm-PAI gene for each PIDS. There were 548 independent

252 eQTLs located in the PIDS regions of the Pm-PAI genes, significantly higher than ($P < 0.001$) the
253 mean of a null distribution (mean = 415) generated by randomly resampling distance-matched
254 pairs of DNAm sites used in the SMR analysis (**Fig. 5a**). These results again imply the regulatory
255 role of the PIDSs in transcription through eQTLs and provide evidence supporting the functional
256 role of the predicted PAIs.
257
258 There were examples where a cis-eQTL was located in a PIDS region predicted to interact with
259 the promoters of multiple genes. For instance, a cis-eQTL was located in an enhancer predicted to
260 interact with the promoters of three genes (i.e., *ABCB9*, *ARL6IP4*, and *MPHOSPH9*) (**Fig. S7**), and
261 the predicted interactions were consistent with the TADs identified by Hi-C from Rao *et al.*[21] (**Fig.
262 S3b**). Furthermore, the predicted interactions between promoters of *ARL6IP4* and *MPHOSPH9* are
263 consistent with the chromatin contact loops identified by Hi-C in the GM12878 cells[21] (**Fig. S7**).
264 The eQTL association signals were highly consistent for the three genes, and the pattern was also
265 consistent with the SNP association signals for schizophrenia (SCZ) and years of education (EY)
266 as shown in our previous work[19], suggesting a plausible mechanism whereby the SNP effects on
267 SCZ and EY are mediated by the expression levels of at least one of the three co-regulated genes
268 through the interactions of the enhancer and three promoters (**Fig. S7**).
269
270 We have shown previously that the functional association between a DNAm site and a gene nearby
271 can be inferred by the pleiotropic association analysis using SMR & HEIDI considering the DNAm
272 level of a CpG site as the exposure and gene expression level as the outcome[19]. We further tested
273 if the PIDSs are enriched among the DNAm sites showing pleiotropic associations with the
274 expression levels of the neighboring Pm-PAI genes. We found that approximately 15% of the
275 PIDSs were the gene-associated DNAm sites identified in our previous study[19], significantly higher
276 ($P < 0.001$) than that computed from the distance-matched control probe pairs (1.3%) described
277 above (**Fig. 5b**).
278
279 **Replication of the predicted PAIs across tissues**
280 To investigate the robustness of the predicted PAIs across tissues, we performed the PAI analysis
281 using brain mQTL data from the Religious Orders Study and Memory and Aging Project
282 (ROSMAP)[34] (n = 468). Of the 11,082 PAIs with $P_{SMR} < 1.76 \times 10^{-9}$ and $P_{HEIDI} > 0.01$ in blood and
283 available in brain, 2,940 (26.5%) showed significant PAIs in brain after Bonferroni correction for
284 multiple testing ($P_{SMR} < 4.51 \times 10^{-6}$ and $P_{HEIDI} > 0.01$). If we use a less stringent threshold for
285 replication, e.g., the nominal P value of 0.05, 66.31% of PAIs predicted in blood were replicated in
286 brain. Here, the replication rate is computed based on a P value threshold, which is dependent of
287 the sample size of the replication data. Alternatively, we can estimate the correlation of PAI effects

288 (i.e., the effect of the exposure DNAm site on the outcome site of a predicted PAI) between brain
289 and blood using the r_b method[35]. This method does not rely on a *P* value threshold and accounts
290 for estimation errors in the estimated effects, which is therefore not dependent of the replication
291 sample size. The estimate of r_b was 0.527 (SE = 0.0051) for 11,082 PAIs between brain and blood,
292 suggesting a relatively strong overlap in PAI between brain and blood.
293
294 It is of note that among the 2,940 blood PAIs replicated at $P_{SMR} < 4.51 \times 10^{-6}$ and $P_{HEIDI} > 0.01$ in
295 brain, there were 268 PAIs for which the PAI effects in blood were in opposite directions to those
296 in brain (**Supplementary Table 2**). For example, the estimated PAI effect between the *SORT1* and
297 *SYPL2* loci was 0.49 in blood and -0.86 in brain. This tissue-specific effect is supported by the
298 differences in gene expression correlation (correlation of expression levels between *SORT1* and
299 *SYPL2* was -0.07 in whole blood and -0.37 in brain frontal cortex; $P_{difference} = 0.0018$) and the
300 chromatin state of the promoter of *SYPL2* (bivalent promoter in blood and active promoter in
301 brain; **Fig. S8**) between brain and blood. Taken together, while there are tissue-specific PAIs, a
302 substantial proportion of the predicted PAIs in blood are consistent with those in brain.
303
304 **Putative target genes of the disease-associated PIDSs**
305 We have shown above the potential functional roles of the predicted PAIs in transcriptional
306 regulation. We then turned to ask how the predicted PAIs can be used to infer the genetic and
307 epigenetic regulatory mechanisms at the GWAS loci for complex traits and diseases. We have
308 previously reported 1,203 pleiotropic associations between 1,045 DNAm sites and 15 complex
309 traits and diseases by an integrative analysis of mQTL, eQTL and GWAS data using the SMR &
310 HEIDI approach[19]. Of the 1,045 trait-associated DNAm sites, 601 (57.5%) sites were involved in
311 the predicted PAIs related to 299 Pm-PAI genes (**Supplementary Table 3**). We first tested the
312 enrichment of the Pm-PAI genes of the trait-associated PIDSs using FUMA[36]. For the 15 complex
313 traits analysed in Wu *et al.*[19], our FUMA analyses identified enrichment in multiple GO and KEGG
314 pathways relevant to the corresponding phenotypes such as the inflammatory response pathway
315 for Crohn's disease (CD) and steroid metabolic process for body mass index (BMI)
316 (**Supplementary Table 4**), demonstrating the regulatory role of the trait-associated PIDSs in
317 biological processes and tissues relevant to the trait or disease.
318
319 There were a number of examples where the predicted PAIs provided important insights to the
320 functional genes underlying the GWAS loci and the underlying mechanisms by which the DNA
321 variants affect the trait through genetic regulation of gene expression. One notable example was
322 a PIDS (cg00271210) in an enhancer region predicted to interact in 3D space with the promoter
323 regions of two genes (i.e., *RNASET2* and *RPS6KA2*), the expression levels of both of which were

324 associated with ulcerative colitis (UC) and CD as reported in our previous study[19] (**Fig. 6**). The
325 SNP-association signals were consistent across CD GWAS, eQTL, and mQTL studies, suggesting
326 that the genetic effect on CD is likely to be mediated through epigenetic regulation of gene
327 expression. Our predicted PAIs further implicated a plausible mechanism whereby the expression
328 levels of *RNASET2* and *RPS6KA2* are co-regulated through the interactions of their promoters with
329 a shared enhancer (**Fig. 6**), although only 41.5% of the predicted PAIs in this region overlapped
330 with the TADs identified by Hi-C from the Rao *et al.* study[21] (**Fig. S3a**) as mentioned above.
331 According to the functional annotation data derived from the REMC samples, it appears that this
332 shared enhancer is highly tissue-specific and present only in B cell and digestive system that are
333 closely relevant to CD (**Fig. 6**). The over-expression of *RNASET2* in spleen (**Fig. S9**) is an additional
334 piece of evidence supporting the functional relevance of this gene to CD. Another interesting
335 example is the *ATG16L1* locus (**Fig. S10**). We have shown previously that five DNAm sites are in
336 pleiotropic associations with CD and the expression level of *ATG16L1*[19]. Of these five DNAm sites,
337 three were in an enhancer region and predicted to interact in 3D space with two DNAm sites in
338 the promoter region of *ATG16L1* (**Fig. S10**), suggesting a plausible mechanism that the genetic
339 effect on CD at this locus is mediated by genetic and epigenetic regulation of the expression level
340 of *ATG16L1* through promoter–enhancer interactions.
341
342 **Discussion**
343 We have presented an analytical approach on the basis of the recently developed SMR & HEIDI
344 method to predict promoter-anchored chromatin interactions using mQTL summary data. The
345 proposed approach uses DNAm level of a CpG site in the promoter region of a gene as the bait to
346 detect its pleiotropic associations with DNAm levels of the other CpG sites (**Fig. 1**) within 2 Mb
347 distance of the focal promoter in either direction. In contrast to experimental assays, such as Hi-
348 C and PCHi-C, our approach is cost-effective (because of the reuse of data available from
349 experiments not originally designed for this purpose) and scalable to large sample sizes. Our
350 method utilises a genetic model to perform a Mendelian randomization analysis so that the
351 detected associations are not confounded by non-genetic factors, which is also distinct from the
352 methods that predict chromatin interactions from the correlations of chromatin accessibility
353 measures[14,16].
354
355 Using mQTL summary-level data from human peripheral blood (n = 1,980), we predicted 34,797
356 PAIs for the promoter regions of 4,617 genes. We showed that the predicted PAIs were enriched
357 in TADs detected by published Hi-C and PCHi-C assays and that the PIDS regions were enriched
358 with eQTLs of target genes. We also showed that the PIDSs were enriched in enhancers and that
359 the Pm-PAI genes tended to be more actively expressed than matched control genes. These results

360 demonstrate the functional relevance of the predicted PAIs to transcriptional regulation and the
361 feasibility of using data from genetic studies of chromatin status to infer three-dimensional
362 chromatin interactions. The proposed approach is applicable to data from genetic studies of other
363 chromatin features such as histone modification (i.e., hQTL)[37] or chromatin accessibility (caQTL)[29].
364 The flexibility of the method also allowed us to analyse data from different tissues or cell types.
365 Using summary data from a brain mQTL study (n = 468), we replicated 26.5% of blood PAIs in
366 brain at a very stringent threshold ($P_{SMR} < 0.05 / m$ with m being the number of tests in the
367 replication set and $P_{HEIDI} > 0.01$) and 66.31% at a less stringent threshold ($P_{SMR} < 0.05$). Together
368 with an estimate of r_b of 0.527 for the correlation of PAI effects between brain and blood, we
369 demonstrated a substantial overlap of the predicted PAIs between blood and brain, in line with
370 the finding from a recent study that cis-mQTLs are largely shared between brain and blood[35].
371
372 The use of a genetic model to detect PAIs also facilitated the integration of the predicted PAIs with
373 GWAS data. In a previous study, Wu *et al.*[19] mapped DNAm sites to genes and then to a trait by
374 checking the consistency of pleiotropic association signals across all the three layers. In this study,
375 we have shown examples of how to integrate the predicted PAIs with GWAS, eQTL and functional
376 annotation data to better understand the genetic and epigenetic regulatory mechanisms
377 underlying the GWAS loci for complex traits (**Figs. 6**, **S7**, and **S10**). The pleiotropic associations
378 between DNAm sites involved in PAIs and a complex trait are also helpful to link genes to the trait
379 at GWAS loci even in the absence of eQTL data. If both DNAm sites of a PAI show pleiotropic
380 association with the trait, the corresponding Pm-PAI gene is likely to be a functionally relevant
381 gene of the trait. Of the 1,045 DNAm sites that showed pleiotropic associations with 15 complex
382 traits as reported in Wu *et al.*[19], 601 sites were involved in the PAIs for 299 Pm-PAI genes
383 identified in this study. In this case, these Pm-PAI genes are very likely to be the functionally
384 relevant genes at the GWAS loci. In comparison with 66 gene targets identified in Wu *et al.*[19]
385 (34/66 overlapped with 299 Pm-PAI genes), integration of PAIs with GWAS facilitates the
386 discovery of more putative gene targets for complex traits.
387
388 There are several reasons why the overlaps between the predicted PAIs and Hi-C loops were
389 limited. First, Hi-C loops were detected with errors. We observed that the concordances between
390 different Hi-C data sets were very limited (**Fig. S11**), consistent with the conclusion from Forcato
391 *et al.* that the reproducibility of Hi-C loops is low at all resolutions[38]. Second, most (65%) of our
392 predicted PAIs are interactions between DNAm sites within 50 Kb (**Fig. S2b**), which are often not
393 well captured by the 3C-based methods due to its low resolution[17]. Third, the chromatin
394 interactions are cell type specific[5] so that differences between the Hi-C loops identified in cell lines
395 and our PAIs identified in whole blood are expected. For the PAIs that were between DNAm sites

396 not located in TADs or Hi-C loops, we have shown specific examples that these predicted PAIs are
397 likely to be functionally interacted (**Fig. 2d and Fig. S3**), suggesting that these PAIs are likely to
398 be interactions yet to be identified by experimental assays. On the other hand, compared to the
399 loops identified based on 3C-based methods, our predicted PAIs are more likely to be functional
400 interactions due to the use of genetic and regulatory epigenomic data, as evidenced by the
401 observation that our predicted Pm-PAI genes showed stronger enrichment in active gene groups
402 compared to the predicted target genes from the PCHi-C data (**Fig. S6**).
403
404 There are some limitations of this study. First, chromatin interactions are likely to be tissue- and
405 temporal-specific whereas our PAI analyses were limited to mQTL data from blood and brain
406 owing to data availability and thus were unable to detect PAIs in specific tissues or at different
407 developmental stages. Second, although the sample size of our blood mQTL summary data is large
408 (n = ~2,000), the PAI analysis could be underpowered if the proportion of variance in exposure
409 or outcome explained by the top associated cis-mQTL is small. Third, the predicted PAIs are
410 relatively sparse as illustrated in **Fig. 2d** because of the sparsity of the DNAm array used, the
411 underlying hypothesis of the SMR method, and the stringent statistical significance level used to
412 claim significant PAIs (**Supplementary Note 1**). Fourth, the functional annotation data derived
413 from the REMC samples could potentially include noise due to the small sample sizes, leading to
414 uncertainty in defining the bait promoter regions. Fifth, if the DNAm levels of two CpG sites are
415 affected by two sets of causal variants in very high LD, these two DNAm sites will appear to be
416 associated in the SMR analysis and the power of the HEIDI test to reject such an SMR association
417 will be limited because of the high LD[18,19]. However, this phenomenon is likely to be rare given
418 that most of the promoter-anchored DNAm sites were predicted to interact with multiple DNAm
419 sites which are very unlikely to be all caused by distinct sets of causal variants in high LD. Sixth,
420 the predicted PAIs including those falling in chromatin loops and TAD regions were not
421 necessarily functional interactions and need to be validated by functional assays in the future.
422 Despite these limitations, our study provides a novel computational paradigm to predict PAIs
423 from genetic effects on epigenetic markers with high resolution. Integrating of the predicted PAIs
424 with GWAS, gene expression, and functional annotation data provides novel insights into the
425 regulatory mechanisms underlying GWAS loci for complex traits. The computational framework
426 is general and applicable to other types of chromatin and histone modification data, to further
427 decipher the functional organisation of the genome.
428

429 **Methods**

430 **Predicting PAIs from mQTL data by the SMR and HEIDI analyses**

431 We used summary-level mQTL data to test whether the variation between people in DNAm levels
432 of two CpG sites are associated because of a set of shared causal variants. Mendelian
433 Randomization (MR) is an approach developed to test for the causal effect of an exposure and an
434 outcome using a genetic variant as the instrumental variable[22,23]. Summary-data–based
435 Mendelian Randomization (SMR) is a variant of MR, originally designed to test for association
436 between the expression level of a gene and a complex trait using summary-level data from GWAS
437 and eQTL studies[18] and subsequently applied to test for associations between DNAm and gene
438 expression and between DNAm and complex traits[19]. Here, we applied the SMR analysis to detect
439 associations between DNAm sites. Let x be an exposure DNAm, y be an outcome DNAm, and z be
440 an instrument SNP associated with exposure DNAm (e.g., $P_{\mathrm{mQTL}} < 5 \times 10^{-8}$). The SMR estimate of
441 the effect of exposure DNAm on the outcome DNAm (i.e., $\hat{b}_{xy}$) is the ratio of the estimated effect
442 of instrument on exposure ($\hat{b}_{zx}$) and that on outcome ($\hat{b}_{zy}$), $\hat{b}_{xy} = \hat{b}_{zy}/\hat{b}_{zx}$, where $\hat{b}_{zx}$ and $\hat{b}_{zy}$ are
443 available from the summary-level mQTL data. We specified the DNAm level of a probe within the
444 promoter region of a gene as the exposure and tested its associations with the DNAm levels of
445 other probes (outcomes) within 2 Mb of the exposure probe (**Fig. 1** and **Fig. S1**). Probe pairs in
446 the same promoter region were not included in the analysis. For a pair of probes in two different
447 promoter regions, the one with higher variance explained by its top associated cis-mQTL was used
448 as the exposure and the other one was used as the outcome. The associations passed the SMR test
449 could possibly be due to linkage (i.e., distinct sets of causal variants in LD, one set affecting the
450 exposure and the other set affecting the outcome), which is less of biological interest in
451 comparison with pleiotropy (i.e., the same set of causal variants affecting both the exposure and
452 the outcome). We then applied the HEIDI (heterogeneity in dependent instruments) test to
453 distinguish pleiotropy from linkage. In brief, the HEIDI test was developed to test against the null
454 hypothesis that the two DNAm sites are affected by the same set of causal variants. This is
455 equivalent to testing whether there is a difference between the $\hat{b}_{xy}$ estimated from any mQTL i
456 ($\hat{b}_{xy(i)}$) and that estimated from the top associated mQTL ($\hat{b}_{xy(top)}$). If we define the difference in
457 estimate between $\hat{b}_{xy}$ at mQTL i and that at top associated mQTL as $\hat{d}_i = \hat{b}_{xy(i)} - \hat{b}_{xy(top)}$, then
458 for multiple mQTLs (i.e., top 20 associated mQTLs after pruning out SNPs in very strong LD), we
459 have $\hat{\mathbf{d}} \sim MVN(\mathbf{d}, \mathbf{V})$, where $\hat{\mathbf{d}} = \{\hat{d}_1, \cdots, \hat{d}_{20}\}$ and $\mathbf{V}$ is the covariance matrix that can be estimated
460 using summary-level mQTL data and LD information from a reference panel[18] (e.g., the 1KGP-
461 imputed HRS[24] data). Therefore, we can test the evidence for heterogeneity through evaluating
462 whether $\mathbf{d} = \mathbf{0}$ using an approximate multivariate approach[39]. We rejected the SMR associations
463 with $P_{\mathrm{HEIDI}} < 0.01$. All these analyses have been implemented in the SMR software tool (**URLs**).

464 Because the mQTL data for the exposure and the outcome were obtained from the same sample,
465 we investigated whether the SMR and HEIDI test-statistics were biased by the sample overlap. To
466 this end, we computed the phenotypic correlation between each pair of exposure and outcome
467 probes as well as the variance explained by the top associated cis-mQTL of each exposure probe,
468 and performed the simulation based on these observed distributions (**Supplementary Note 2**).
469 The simulation results showed that *P* values from both SMR and HEIDI tests were evenly
470 distributed under the null model without inflation or deflation (**Fig. S12**). We have made all the
471 PAIs analysis scripts publicly available at GitHub https://github.com/wuyangf7/PAI.
472
473 **Data used for the PAI analysis**
474 The peripheral blood mQTL summary data were from the Brisbane Systems Genetics Study
475 (BSGS)[40] (*n*=614) and Lothian Birth Cohorts (LBC) of 1921 and 1936[41] (*n*=1,366). We performed
476 a meta-analysis of the two cohorts and identified 90,749 DNAm probes with at least a cis-mQTL
477 at $P_{\mathrm{mQTL}} < 5\times10^{-8}$ (excluding the probes in the major histocompatibility complex (MHC) region
478 because of the complexity of this region), of which 28,732 DNAm probes were in the promoter
479 regions defined by the annotation data derived from 23 REMC blood samples (T-cell, B-cell, and
480 Hematopoietic stem cells). The prefrontal cortex mQTL summary data were from the Religious
481 Orders Study and Memory and Aging Project (ROSMAP)[34] (*n*=468), comprising 419,253 probes
482 and approximate 6.5 million genetic variants. In the ROSMAP data, there were 67,995 DNAm
483 probes with at least a cis-mQTL at $P_{\mathrm{mQTL}} < 5\times10^{-8}$ (not including the probes in the MHC region), of
484 which 22,285 DNAm probes were in the promoter regions defined by the annotation data derived
485 from 10 REMC brain samples. For all the DNAm probes, enhanced annotation data from Price *et*
486 *al.*[42] (**URLs**) were used to annotate the closest gene of each DNAm probe.
487
488 We included in the analysis 15 complex traits (including disease) as analysed in Wu *et al.*[19]. They
489 are height[43], body mass index (BMI)[44], waist-hip-ratio adjusted by BMI (WHRadjBMI)[45], high-
490 density lipoprotein (HDL)[46], low-density lipoprotein (LDL)[46], thyroglobulin (TG)[46], educational
491 years (EY)[47], rheumatoid arthritis (RA)[48], schizophrenia (SCZ)[49], coronary artery disease (CAD)[50],
492 type 2 diabetes (T2D)[51], Crohn's disease (CD)[52], ulcerative colitis (UC)[52], Alzheimer's disease
493 (AD)[53] and inflammatory bowel disease (IBD)[52]. The GWAS summary data were from the large
494 GWAS meta-analyses (predominantly in samples of European ancestry) with sample sizes of up
495 to 339,224. The number of SNPs varied from 2.5 to 9.4 million across traits.
496
497 **Annotations of the chromatin state**
498 The epigenomic annotation data used in this study were from the Roadmap Epigenomics Mapping
499 Consortium (REMC), publicly available at http://compbio.mit.edu/roadmap/. We used these data

500 to annotate the functional relevance of the DNAm sites and their cell type or tissue specificity. The
501 chromatin state annotations from the Roadmap Epigenomics Project[13] were predicted by
502 ChromHMM[12] based on the imputed data of 12 histone-modification marks. It contains 25
503 functional categories for 127 epigenomes in a wide range of primary tissue and cell types (**URLs**).
504 The 25 chromatin states were further combined into 14 main functional annotations (as shown
505 in **Fig. 4b** and Wu *et al.*[19]).
506
507 **Overlap of the predicted PAIs with Hi-C, PCHi-C and ChIA-PET data**
508 To test the overlap between our predicted PAIs and chromatin contacts detected by Hi-C, PCHi-C
509 or ChIA-PET, we used chromatin contact loops and topological associated domains (TADs) data
510 from the Rao *et al.* study called in the GM12812 cells[21] and the Dixon *et al.* study in embryonic
511 stem cells[26], PCHi-C interaction data generated from human primary hematopoietic cells[5], and the
512 *POLR2A* ChIA-PET chromatin loops from the ENCODE project[27] (**Supplementary Table 1**). To
513 assess the statistical significance of the enrichment, we generated a null distribution by randomly
514 sampling 1,000 sets of control probe pairs (with the same number as that of the predicted PAIs)
515 from the distance-matched probe pairs tested in the SMR analysis. We mapped both the predicted
516 PAIs and the control probe pairs to the TAD regions or chromatin contact loops detected by
517 previous experimental assays and quantified the number of overlapping pairs. We estimated the
518 fold enrichment by the ratio of the overlapping number for the predicted PAIs to the mean of the
519 null distribution and computed the empirical *P* value by comparing the overlapping number for
520 the predicted PAIs with the null distribution.
521
522 We used the chromatin interaction data generated by Jung *et al.*[28] in GM12878 cell lines as a
523 validation set to evaluate the performance of different interaction prediction methods. We
524 quantified the enrichment of the predicted interactions by different methods in the significant
525 PCHi-C loops defined based on a range of PCHi-C *P* value thresholds and used the Fisher's exact
526 test to assess the statistical significance of the enrichment.
527
528 **Enrichment of the PIDSs in functional annotations**
529 To conduct an enrichment test of the promoter interacting DNAm sites (PIDSs) in different
530 functional annotation categories, we first extracted chromatin state data of 23 blood samples from
531 the REMC samples. We then mapped the PIDSs to 14 main functional categories based on the
532 physical positions, and counted the number of PIDSs in each functional category. Again, we
533 generated a null distribution by randomly sampling the same number of control probes (with
534 variance in DNAm level matched with the PIDSs) from all the probes tested in the PAI analysis and
535 repeated the random sampling 1,000 times. The fold enrichment was calculated by the ratio of the

536 observed value to the mean of the null distribution, and an empirical *P* value was computed by
537 comparing the observed value with the null distribution.
538
539 **Quantifying the expression levels of Pm-PAI genes**
540 To quantify the expression levels of genes whose promoters were involved in the predicted PAIs
541 (Pm-PAI genes), we used gene expression data (measured by Transcript Per Kilobase Million
542 mapped reads (TPM)) from blood samples of the Genotype-Tissue Expression (GTEx) project[32].
543 We classified all the genes into two groups based on their expression levels in GTEx blood, i.e.,
544 active and inactive (TPM < 0.1). For the active genes, we further divided them into four quartiles
545 based on their expression levels in GTEx blood, and counted the number of Pm-PAI genes in each
546 of the five groups. To generate the null distribution, we randomly sampled the same number of
547 control genes whose promoter DNAm sites were included in the SMR analysis, and repeated the
548 random sampling 1,000 times. We computed the number of Pm-PAI genes and control genes in
549 each group and assessed the significance by comparing the number of Pm-PAI genes with the null
550 distribution in each group. We further tested the enrichment of the Pm-PAI genes against a null
551 distribution sampled from all genes.
552
553 **Enrichment of eQTLs and gene-associated DNAm in the PIDS regions**
554 The eQTL enrichment analysis was conducted using all the independent cis-eQTLs (m=11,204)
555 from the CAGE[33] study. The independent cis-eQTLs were from SNP-probe associations ($P < 5\times10^{-8}$)
556 after clumping analysis in PLINK[54] followed by a conditional and joint (COJO) analysis in GCTA[55].
557 We only retained the cis-eQTLs whose target genes had at least a PIDS and mapped the cis-eQTL
558 to a 10 Kb region centred around each corresponding PIDS of a Pm-PAI gene. To assess the
559 significance of the enrichment, we generated a null distribution by mapping the cis-eQTLs to the
560 same number of control gene-DNAm pairs (strictly speaking, it is the bait DNAm probe in the
561 promoter of a gene together with another non-promoter DNAm probe) randomly sampled (with
562 1,000 repeats) from those included in the PAI analysis with the distance between a control pair
563 matched with that between a Pm-PAI gene and the corresponding PIDS. In addition, we have
564 identified a set of DNAm sites that showed pleiotropic associations with gene expressions in a
565 previous study[19]. We used the same approach as described above to test the significance of
566 enrichment of the gene-associated DNAm sites in the PIDSs.
567
568 **Supplemental information**
569 Supplemental data include 12 supplemental figures and 4 supplemental tables.
570
571 **URLs**

572 M2Mdb, http://cnsgenomics.com/shiny/M2Mdb/
573 SMR, http://cnsgenomics.com/software/smr
574 GTEx, http://www.gtexportal.org/home/
575 Annotation file for the Illumina HumanMethylation450 BeadChip,
576 https://www.ncbi.nlm.nih.gov/geo/query/acc.cgi?acc=GPL16304
577

578 **Acknowledgements**

579 We thank Peter Visscher for helpful discussion. This research was supported by the Australian
580 Research Council (DP160101343, DP160101056 and FT180100186), the Australian National
581 Health and Medical Research Council (1107258, 1083656, 1078901 and 1113400), and the Sylvia
582 & Charles Viertel Charitable Foundation. The Lothian Birth Cohorts (LBC) are supported by Age
583 UK (Disconnected Mind programme). Methylation typing was supported by Centre for Cognitive
584 Ageing and Cognitive Epidemiology (Pilot Fund award), Age UK, The Wellcome Trust Institutional
585 Strategic Support Fund, The University of Edinburgh, and The University of Queensland. The LBC
586 resource is prepared in the Centre for Cognitive Ageing and Cognitive Epidemiology, which is
587 supported by the Medical Research Council and Biotechnology and Biological Sciences Research
588 Council (MR/K026992/1), and which supports I.J.D.. This study makes use of data from dbGaP
589 (accessions**:** phs000428.v1.p1 and phs000424.v1.p1) and EGA (accession: EGAS00001000108).
590 A full list of acknowledgements to these data sets can be found in the **Supplementary Note 3**.
591

592 **Author Contributions**

593 J.Y. conceived and supervised the study. Y.W., T.Q. and J.Y. designed the experiment. Y.W. and T.Q.
594 performed simulations and statistical analyses under the assistance or guidance from J.Y., J.Z.,
595 H.W., F.Z., and Z.Z.. I.J.D., N.R.W. and A.F.M. contributed the blood DNA methylation data. J.E.P.C.
596 provided critical advice that significantly improved the interpretation of the results. N.R.W. and
597 J.Y. contributed funding and resources. Y.W., T.Q., J.Z. and J.Y. wrote the manuscript with the
598 participation of all authors.
599

600 **Declaration of Interests**

601 We declare that all authors have no competing interests.
602

603 **References**

604 1. MacArthur, J. *et al.* The new NHGRI-EBI Catalog of published genome-wide association
605 studies (GWAS Catalog). *Nucleic Acids Research* **45**, D896-D901 (2017).
606 2. Visscher, P.M. *et al.* 10 Years of GWAS Discovery: Biology, Function, and Translation. *Am J*
607 *Hum Genet* **101**, 5-22 (2017).

608 3. Farh, K.K.-H. *et al.* Genetic and epigenetic fine mapping of causal autoimmune disease
609 variants. *Nature* **518**, 337-343 (2015).
610 4. Claussnitzer, M. *et al.* FTO Obesity Variant Circuitry and Adipocyte Browning in Humans.
611 *New England Journal of Medicine* **373**, 895-907 (2015).
612 5. Javierre, B.M. *et al.* Lineage-Specific Genome Architecture Links Enhancers and Non-
613 coding Disease Variants to Target Gene Promoters. *Cell* **167**, 1369-1384 e19 (2016).
614 6. Khurana, E. *et al.* Role of non-coding sequence variants in cancer. *Nat Rev Genet* **17**, 93-
615 108 (2016).
616 7. Lieberman-Aiden, E. *et al.* Comprehensive Mapping of Long-Range Interactions Reveals
617 Folding Principles of the Human Genome. *Science* **326**, 289-293 (2009).
618 8. Fullwood, M.J. *et al.* An oestrogen-receptor-alpha-bound human chromatin interactome.
619 *Nature* **462**, 58-64 (2009).
620 9. Wit, E.d. & Laat, W.d. A decade of 3C technologies: insights into nuclear organization.
621 *Genes & Development* **26**, 11-24 (2012).
622 10. Kuo, M.-H. & Allis, C.D. In Vivo Cross-Linking and Immunoprecipitation for Studying
623 Dynamic Protein:DNA Associations in a Chromatin Environment. *Methods* **19**, 425-433
624 (1999).
625 11. Belton, J.M. *et al.* Hi-C: a comprehensive technique to capture the conformation of
626 genomes. *Methods* **58**, 268-76 (2012).
627 12. Ernst, J. & Kellis, M. ChromHMM: automating chromatin-state discovery and
628 characterization. *Nat Methods* **9**, 215-6 (2012).
629 13. Roadmap Epigenomics Consortium *et al.* Integrative analysis of 111 reference human
630 epigenomes. *Nature* **518**, 317-30 (2015).
631 14. Zhu, Y. *et al.* Constructing 3D interaction maps from 1D epigenomes. *Nat Commun* **7**,
632 10812 (2016).
633 15. Huang, J., Marco, E., Pinello, L. & Yuan, G.-C. Predicting chromatin organization using
634 histone marks. *Genome Biology* **16**, 162 (2015).
635 16. Fortin, J.-P. & Hansen, K.D. Reconstructing A/B compartments as revealed by Hi-C using
636 long-range correlations in epigenetic data. *Genome Biology* **16**, 180 (2015).
637 17. Kumasaka, N., Knights, A.J. & Gaffney, D.J. High-resolution genetic mapping of putative
638 causal interactions between regions of open chromatin. *Nature Genetics* **51**, 128-137
639 (2019).
640 18. Zhu, Z. *et al.* Integration of summary data from GWAS and eQTL studies predicts complex
641 trait gene targets. *Nat Genet* **48**, 481-7 (2016).
642 19. Wu, Y. *et al.* Integrative analysis of omics summary data reveals putative mechanisms
643 underlying complex traits. *Nature Communications* **9**, 918 (2018).

644 20. McRae, A.F. *et al.* Identification of 55,000 Replicated DNA Methylation QTL. *Scientific*
645 *Reports* **8**, 17605 (2018).
646 21. Rao, Suhas S.P. *et al.* A 3D Map of the Human Genome at Kilobase Resolution Reveals
647 Principles of Chromatin Looping. *Cell* **159**, 1665-1680 (2014).
648 22. Davey Smith, G. & Hemani, G. Mendelian randomization: genetic anchors for causal
649 inference in epidemiological studies. *Human Molecular Genetics* **23**, R89-R98 (2014).
650 23. Davey Smith, G. & Ebrahim, S. 'Mendelian randomization': can genetic epidemiology
651 contribute to understanding environmental determinants of disease? *International*
652 *Journal of Epidemiology* **32**, 1-22 (2003).
653 24. Sonnega, A. *et al.* Cohort Profile: the Health and Retirement Study (HRS). *Int J Epidemiol*
654 **43**, 576-85 (2014).
655 25. Pombo, A. & Dillon, N. Three-dimensional genome architecture: players and mechanisms.
656 *Nat Rev Mol Cell Biol* **16**, 245-57 (2015).
657 26. Dixon, J.R. *et al.* Topological domains in mammalian genomes identified by analysis of
658 chromatin interactions. *Nature* **485**, 376-80 (2012).
659 27. Consortium, E.P. An integrated encyclopedia of DNA elements in the human genome.
660 *Nature* **489**, 57-74 (2012).
661 28. Jung, I. *et al.* A compendium of promoter-centered long-range chromatin interactions in
662 the human genome. *Nat Genet* **51**, 1442-1449 (2019).
663 29. Gate, R.E. *et al.* Genetic determinants of co-accessible chromatin regions in activated T
664 cells across humans. *Nat Genet* **50**, 1140-1150 (2018).
665 30. Jin, F. *et al.* A high-resolution map of the three-dimensional chromatin interactome in
666 human cells. *Nature* **503**, 290 (2013).
667 31. Li, G. *et al.* Extensive Promoter-centered Chromatin Interactions Provide a Topological
668 Basis for Transcription Regulation. *Cell* **148**, 84-98 (2012).
669 32. The GTEx Consortium. The Genotype-Tissue Expression (GTEx) pilot analysis:
670 Multitissue gene regulation in humans. *Science* **348**, 648-660 (2015).
671 33. Lloyd-Jones, L.R. *et al.* The Genetic Architecture of Gene Expression in Peripheral Blood.
672 *Am J Hum Genet* **100**, 371 (2017).
673 34. Ng, B. *et al.* An xQTL map integrates the genetic architecture of the human brain's
674 transcriptome and epigenome. *Nature Neuroscience* **20**, 1418 (2017).
675 35. Qi, T. *et al.* Identifying gene targets for brain-related traits using transcriptomic and
676 methylomic data from blood. *Nature Communications* **9**, 2282 (2018).
677 36. Watanabe, K., Taskesen, E., van Bochoven, A. & Posthuma, D. Functional mapping and
678 annotation of genetic associations with FUMA. *Nature Communications* **8**, 1826 (2017).

679 37. Chen, L. *et al.* Genetic Drivers of Epigenetic and Transcriptional Variation in Human
680 Immune Cells. *Cell* **167**, 1398-1414 e24 (2016).
681 38. Forcato, M. *et al.* Comparison of computational methods for Hi-C data analysis. *Nat*
682 *Methods* **14**, 679-685 (2017).
683 39. Kuonen, D. Saddlepoint Approximations for Distributions of Quadratic Forms in Normal
684 Variables. *Biometrika* **86**, 929-935 (1999).
685 40. Powell, J.E. *et al.* The Brisbane Systems Genetics Study: genetical genomics meets
686 complex trait genetics. *PLoS One* **7**, e35430 (2012).
687 41. Chen, B.H. *et al.* DNA methylation-based measures of biological age: meta-analysis
688 predicting time to death. *Aging (Albany NY)* **8**, 1844-1865 (2016).
689 42. Price, M.E. *et al.* Additional annotation enhances potential for biologically-relevant
690 analysis of the Illumina Infinium HumanMethylation450 BeadChip array. *Epigenetics*
691 *Chromatin* **6**, 4 (2013).
692 43. Wood, A.R. *et al.* Defining the role of common variation in the genomic and biological
693 architecture of adult human height. *Nat Genet* **46**, 1173-86 (2014).
694 44. Locke, A.E. *et al.* Genetic studies of body mass index yield new insights for obesity
695 biology. *Nature* **518**, 197-206 (2015).
696 45. Shungin, D. *et al.* New genetic loci link adipose and insulin biology to body fat
697 distribution. *Nature* **518**, 187-96 (2015).
698 46. Global Lipids Genetics Consortium *et al.* Discovery and refinement of loci associated with
699 lipid levels. *Nat Genet* **45**, 1274-83 (2013).
700 47. Okbay, A. *et al.* Genome-wide association study identifies 74 loci associated with
701 educational attainment. *Nature* **533**, 539-42 (2016).
702 48. Okada, Y. *et al.* Genetics of rheumatoid arthritis contributes to biology and drug
703 discovery. *Nature* **506**, 376-381 (2014).
704 49. Schizophrenia Working Group of the Psychiatric Genomics Consortium. Biological
705 insights from 108 schizophrenia-associated genetic loci. *Nature* **511**, 421-7 (2014).
706 50. Nikpay, M. *et al.* A comprehensive 1,000 Genomes-based genome-wide association meta-
707 analysis of coronary artery disease. *Nat Genet* **47**, 1121-30 (2015).
708 51. Morris, A.P. *et al.* Large-scale association analysis provides insights into the genetic
709 architecture and pathophysiology of type 2 diabetes. *Nature genetics* **44**, 981 (2012).
710 52. Liu, J.Z. *et al.* Association analyses identify 38 susceptibility loci for inflammatory bowel
711 disease and highlight shared genetic risk across populations. *Nat Genet* **47**, 979-986
712 (2015).
713 53. Lambert, J.C. *et al.* Meta-analysis of 74,046 individuals identifies 11 new susceptibility
714 loci for Alzheimer's disease. *Nat Genet* **45**, 1452-8 (2013).

715 54. Purcell, S. *et al.* PLINK: a tool set for whole-genome association and population-based
716 linkage analyses. *Am J Hum Genet* **81**, 559-75 (2007).
717 55. Yang, J. *et al.* Conditional and joint multiple-SNP analysis of GWAS summary statistics
718 identifies additional variants influencing complex traits. *Nature Genetics* **44**, 369 (2012).
719 56. Grubert, F. *et al.* Genetic Control of Chromatin States in Humans Involves Local and Distal
720 Chromosomal Interactions. *Cell* **162**, 1051-65 (2015).
721

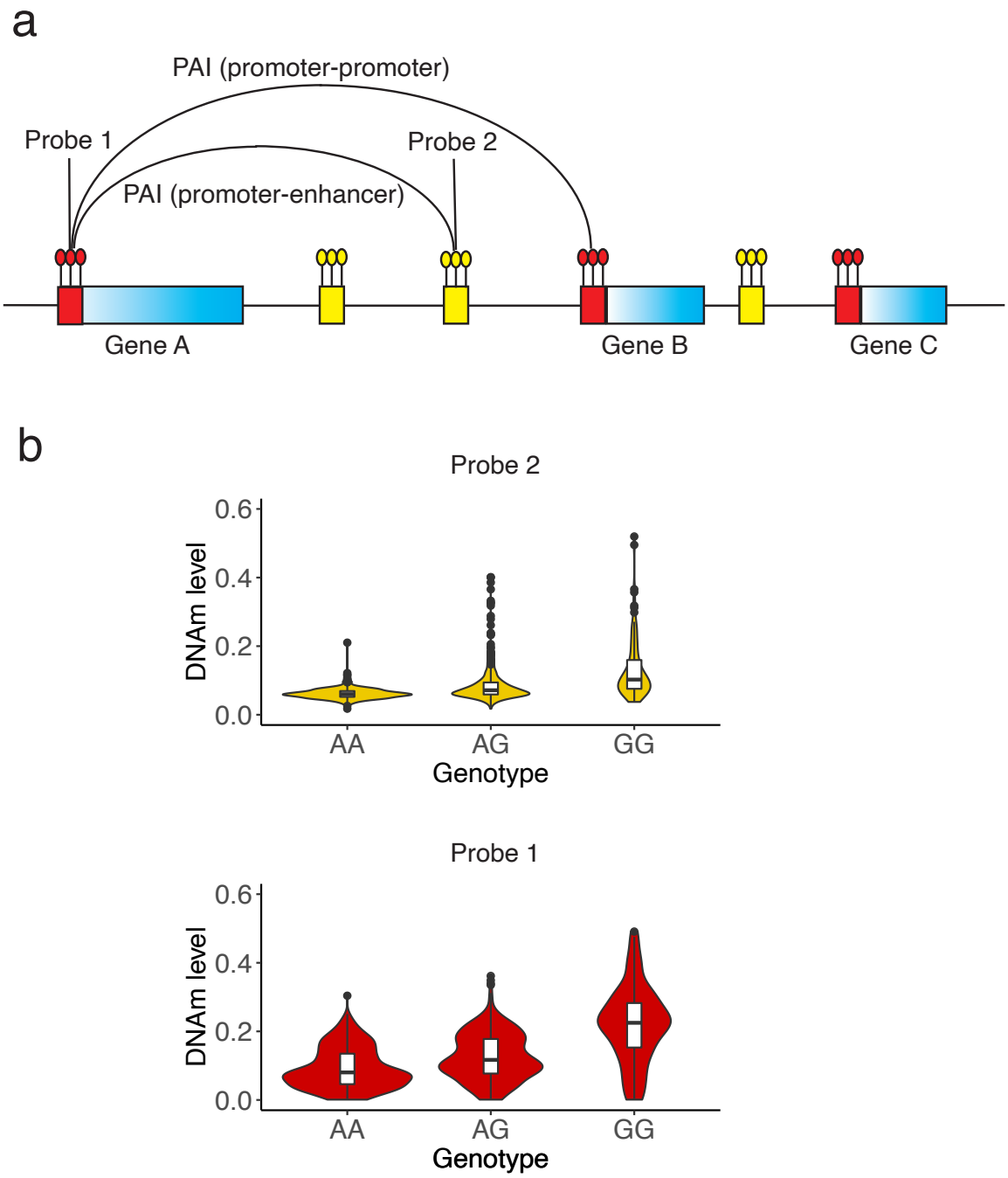

Figure 1 Schematic of the promoter-anchored interaction (PAI) analysis. Panel a): a schematic of the PAI analysis. The blue rectangles represent genes with their promoter regions color coded in red. The small yellow bars represent other functional regions (e.g., enhancers). In this toy example, the promoter region of Gene A is used as the bait for the PAI analysis. Genes (e.g., genes A and B) whose promoters are involved in significant PAIs are defined as Pm-PAI genes. DNAm sites (e.g., DNAm probe 2) that showed significant interactions with the DNAm sites in promoter regions are defined as promoter-interacting DNAm sites or PIDS. Panel b): variation between people in DNAm levels of two CpG sites are associated because of a shared causal variant. The DNAm level ranges

731 from 0 to 1 (with 0 being unmethylated and 1 being fully methylated). It is the ratio of the
732 methylated probe intensity to the overall intensity (sum of methylated and unmethylated probe
733 intensities).
734

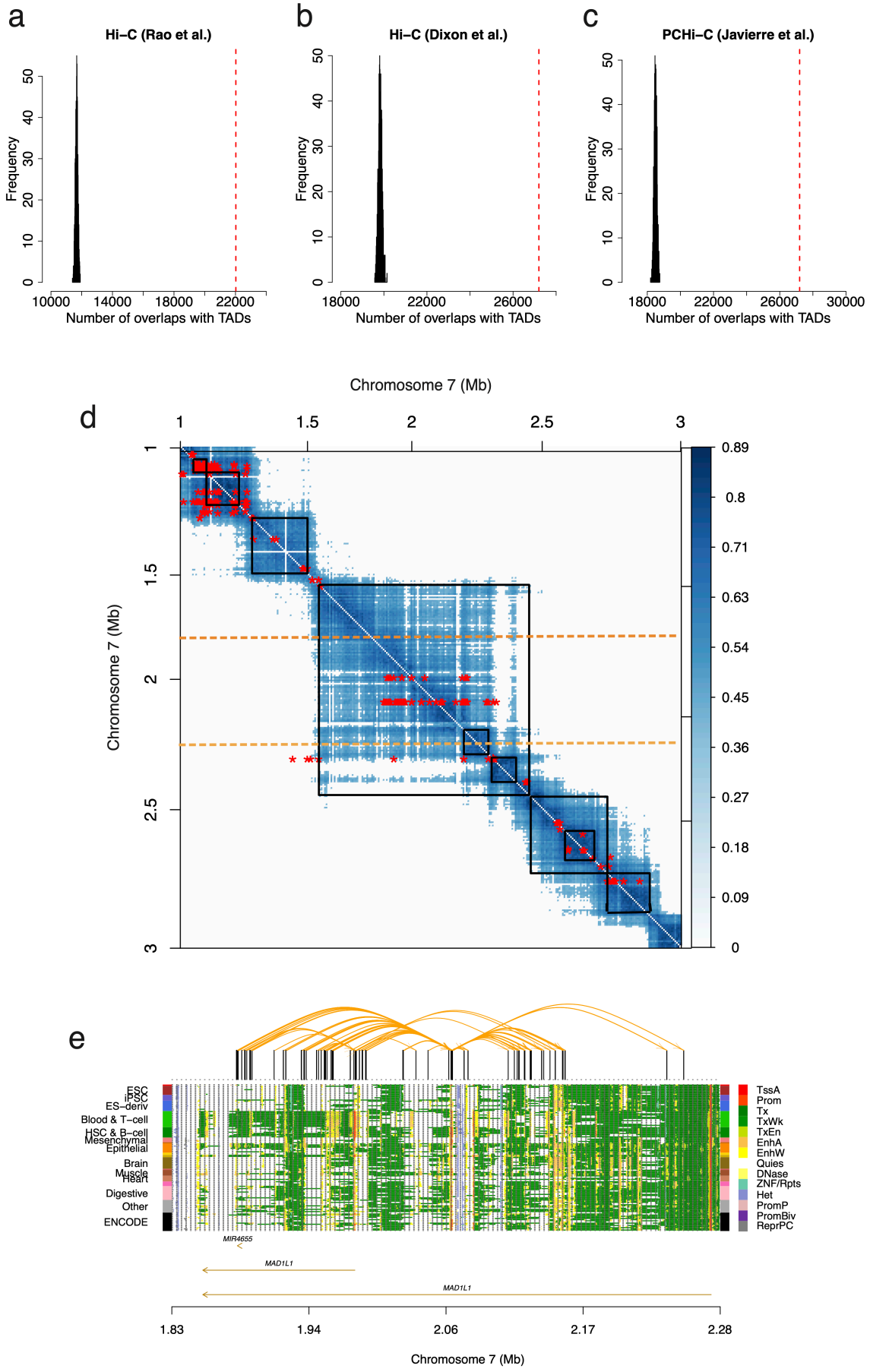
a
Hi–C (Rao et al.)
Frequency
Number of overlaps with TADs
b
Hi–C (Dixon et al.)
Frequency
Number of overlaps with TADs
c
PCHi–C (Javierre et al.)
Frequency
Number of overlaps with TADs
d
Chromosome 7 (Mb)
Chromosome 7 (Mb)
e
ESC
iPSC
ES–deriv
Blood & T–cell
HSC & B–cell
Mesenchymal
Epithelial
Brain
Muscle
Heart
Digestive
Other
ENCODE
TssA
Prom
Tx
TxWk
TxEn
EnhA
EnhW
Quies
DNase
ZNF/Rpts
Het
PromP
PromBiv
ReprPC
MIR4655
MAD1L1
MAD1L1
Chromosome 7 (Mb)

735

736 **Figure 2** Overlap of the predicted PAIs with TADs identified by Hi-C and PCHi-C. Panels a), b) and
737 c): overlaps of the predicted PAIs with TADs identified by a) Rao *et al.*[21] and b) Dixon *et al.*[26] using
738 Hi-C and by c) Javierre *et al.*[5] using PCHi-C. The red dash lines represent the observed number and
739 histograms represent the distribution of control sets. Panel d): a heatmap of the predicted PAIs
740 (red asterisks) and chromatin interactions with correlation scores > 0.4 (blue dots) identified by
741 Grubert *et al.*[56] using Hi-C in a 2 Mb region on chromosome 7. Black squares represent the TADs
742 identified by Rao *et al.*[21]. The heatmap is asymmetric for the PAIs (red asterisks) with the *x*- and
743 *y*-axes representing the physical positions of outcome and exposure DNAm probes, respectively.
744 Panel e): the predicted PAIs at the *MAD1L1* locus, a 450-Kb sub-region of that shown between two
745 orange dashed lines in panel d). The orange curved lines on the top represent the significant PAIs
746 between 14 DNAm sites in the promoter regions of *MAD1L1* (multiple transcripts) and other
747 DNAm sites nearby. The panel on the bottom represents 14 chromatin state annotations
748 (indicated by different colours) inferred from data of 127 REMC samples (one row per sample).
749 Note that the predicted PAIs appear to be much sparser than the Hi-C loops largely because the
750 PAIs were predicted from analyses with very stringent significance levels (**Supplementary Note**
751 **1**).
752
753

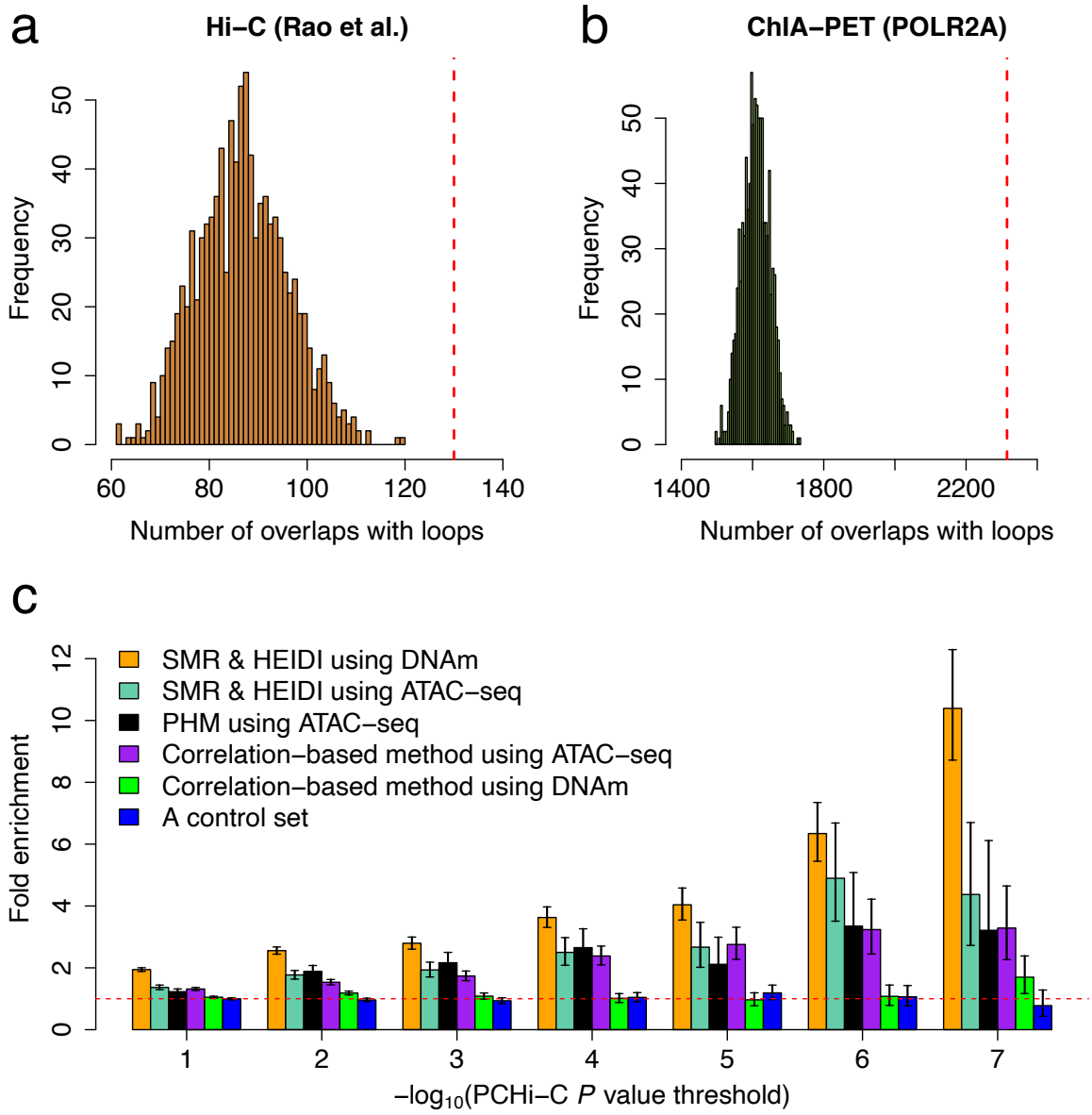

Figure 3 Enrichment of the predicted interactions in chromatin loops identified by experimental assays. Panels a) and b): overlaps of the predicted PAIs with the chromatin loops identified by a) Hi-C from Rao *et al.*[21] and b) *POLR2A* ChIA-PET from the ENCODE project[27]. The red dash lines represent the observed number and histograms represent the distribution of control sets. Panel c): enrichment of the predicted interactions in the significant PCHi-C loops defined based on a range of *P* value thresholds. We used the PCHi-C loops identified from Jung *et al.* in GM12878 cell lines[28]. PHM: the pairwise hierarchical model developed by Kumasaka *et al.*[17]. The error bar around each estimate represents the 95% confidence interval. The horizontal red dashed line indicates no enrichment.

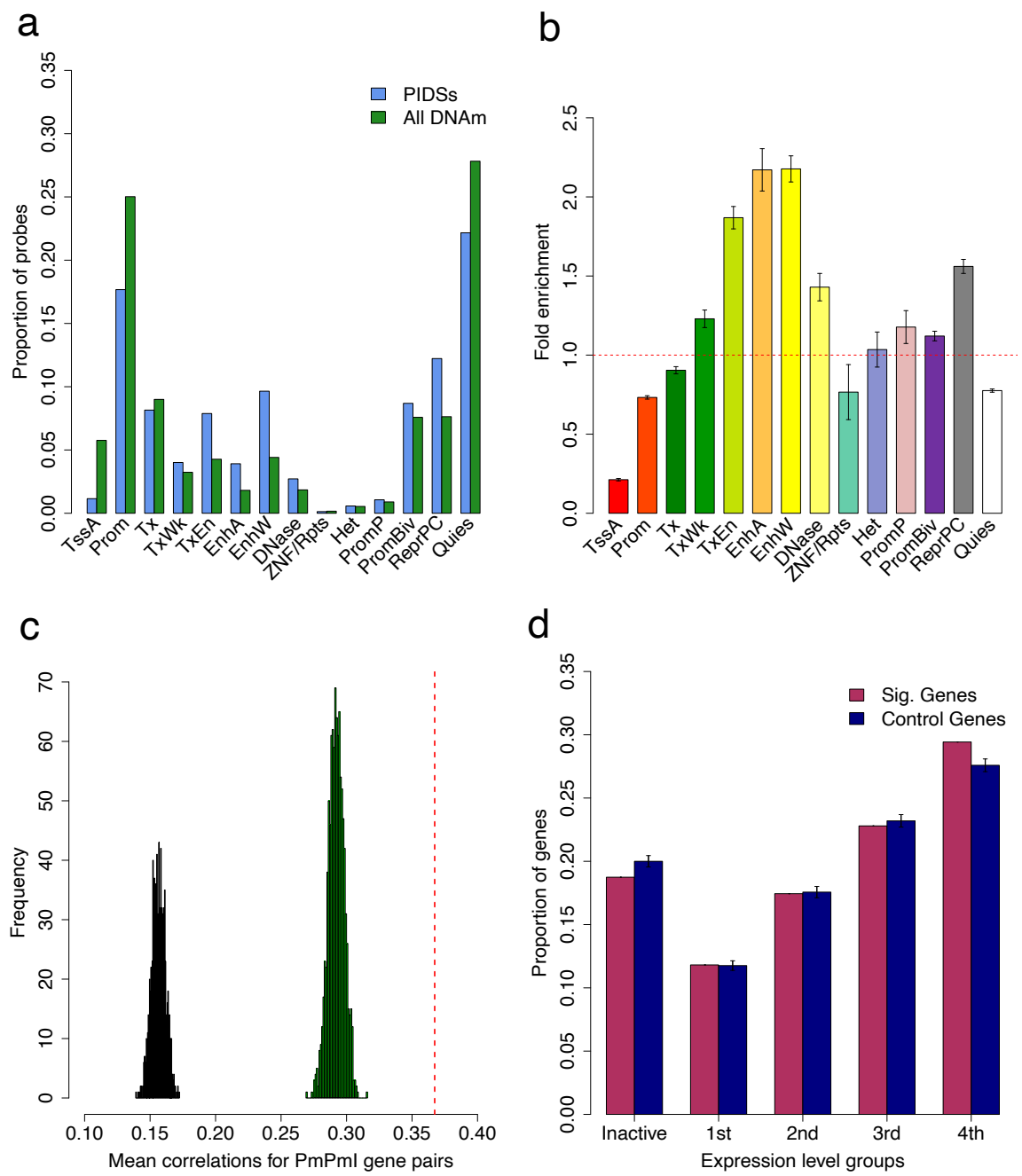

Figure 4 Enrichment of PIDSs and Pm-PAI genes. Panels a) and b): enrichment of PIDSs in 14 main functional annotation categories inferred from the 127 REMC samples. Fold enrichment: a ratio of the proportion of PIDSs in an annotation category to the mean of the control sets. The error bar in panel b) represents standard deviation of the estimate under the null obtained from the control sets. The 14 functional categories are: TssA, active transcription start site; Prom, upstream/downstream TSS promoter; Tx, actively transcribed state; TxWk, weak transcription; TxEn, transcribed and regulatory Prom/Enh; EnhA, active enhancer; EnhW, weak enhancer; DNase, primary DNase; ZNF/Rpts, state associated with zinc finger protein genes; Het, constitutive heterochromatin; PromP, Poised promoter; PromBiv, bivalent regulatory states;

ReprPC, repressed Polycomb states; and Quies, a quiescent state. Panel c): mean Pearson correlation of expression levels for gene pairs whose promoters were involved in PmPmI. The red dash line represents the observed mean Pearson correlation value of the significant PmPmI gene pairs and the histograms represent the null distributions of mean Pearson correlation values generated by repeated resampling of a set of distance-matched control gene pairs either from the genes whose promoters were involved in the SMR analysis (green) or from all genes (black). Panel d): proportion of Pm-PAI genes in five gene activity groups with the first group being the inactive group (TPM <0.1) together with four quartiles defined based on the expression levels of all genes in the GTEx blood samples. The error bar represents the standard deviation estimated from the 1,000 control sets.

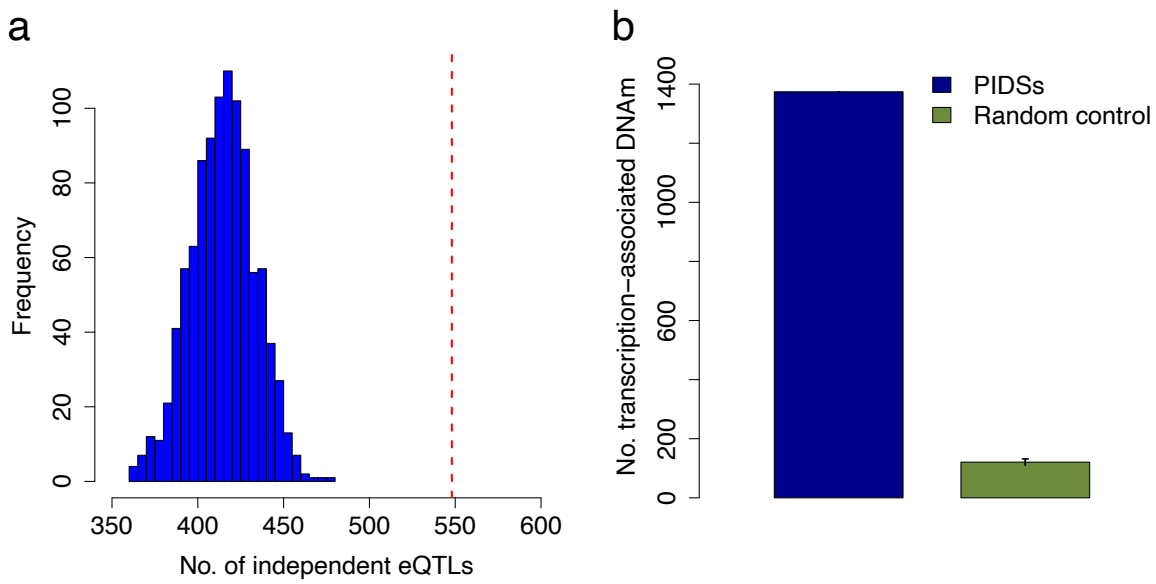

787

788 **Figure 5** Enrichment of eQTLs or transcription-associated DNAm sites in PIDS regions of the Pm-
789 PAI genes. Panel a): the number of independent cis-eQTLs ($P_{\mathrm{eQTL}} < 5\times10^{-8}$) located in PIDS regions
790 of the Pm-PAI genes. The red dash line represents the observed number and the blue histogram
791 represents the distribution of 1000 control sets. Panel b): the number of transcription-associated
792 DNAm sites located in PIDS regions of the Pm-PAI genes. The blue bar represents the observed
793 number and the green bar represents the mean of 1000 control sets. The error bar represents the
794 standard deviation estimated from the control sets.

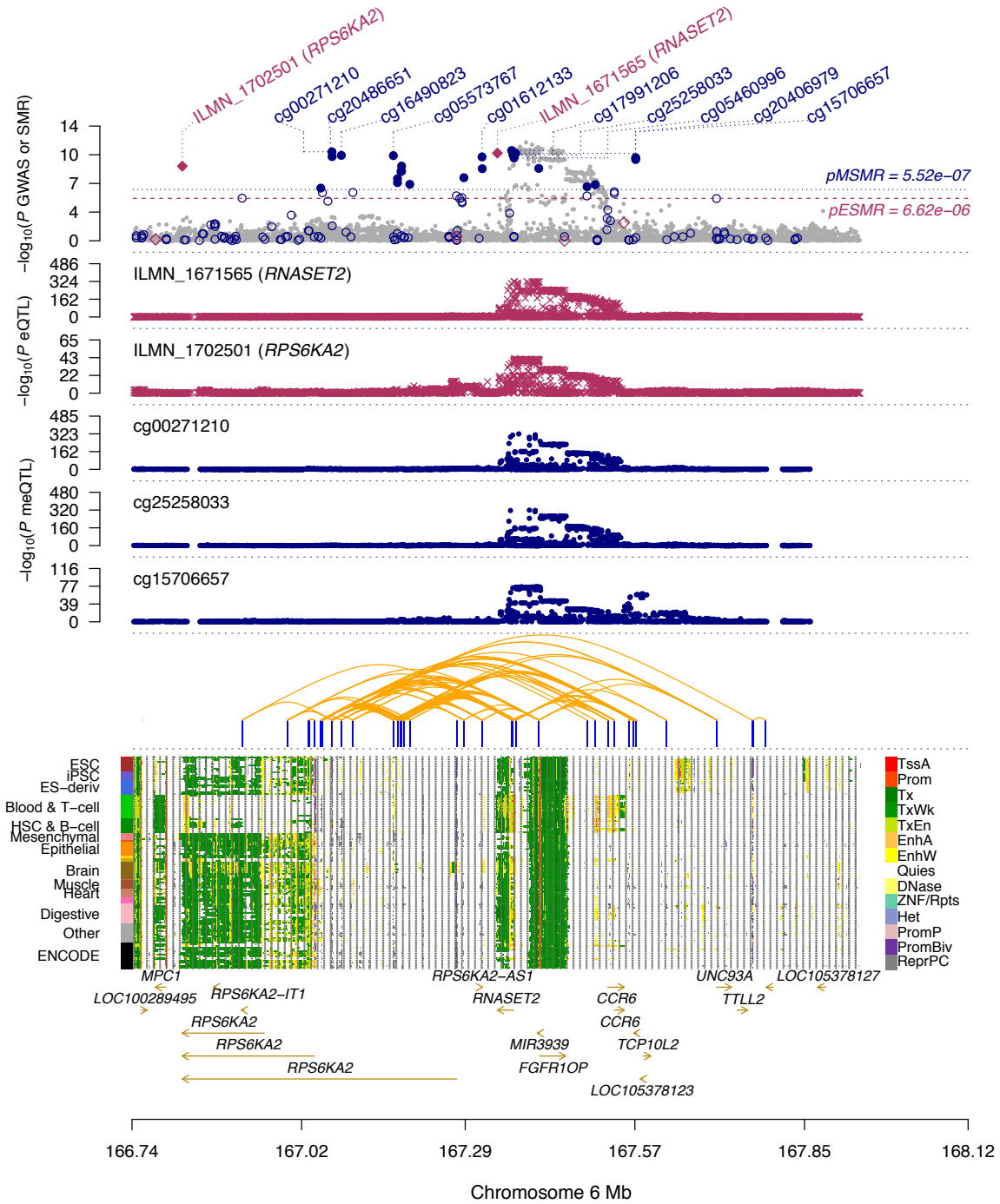

Figure 6 Prioritizing genes and functional regions at the *RPS6KA2* locus for Crohn's disease (CD). The top plot shows -log$_{10}$(*P* values) of SNPs from the GWAS meta-analysis (grey dots) for CD[48]. Red diamonds and blue circles represent -log$_{10}$(*P* values) from SMR tests for associations of gene expression and DNAm probes with CD, respectively. Solid diamonds and circles are the probes not rejected by the HEIDI test (P_{HEIDI}>0.01). The second and third plots show -log$_{10}$(*P* values) of SNP associations for the expression levels of probe ILMN_1671565 (tagging *RNASET2*) and ILMN_1702501 (tagging *RPS6KA2*), respectively, from the CAGE data. The fourth, fifth and sixth plots shows -log$_{10}$(*P* values) of SNP associations for the DNAm levels of probes cg00271210,

804 cg25258033, and cg15706657, respectively, from the mQTL meta-analysis. The panel on the
805 bottom shows 14 chromatin state annotations (indicated by colours) inferred from 127 REMC
806 samples (one sample per row) with the predicted PAIs annotated by orange curved lines on the
807 top (see **Fig. S3a** for the overlap of the predicted PAIs with Hi-C data).